

Nociceptive sensory neurons drive interleukin-23-mediated psoriasiform skin inflammation

Lorena Riol-Blanco^{1*}, Jose Ordovas-Montanes^{1*}, Mario Perro¹, Elena Naval¹, Aude Thiriot¹, David Alvarez¹, John N. Wood² & Ulrich H. von Andrian¹

The skin has a dual function as a barrier and a sensory interface between the body and the environment. To protect against invading pathogens, the skin harbours specialized immune cells, including dermal dendritic cells (DDCs) and interleukin (IL)-17-producing $\gamma\delta$ T ($\gamma\delta$ T17) cells, the aberrant activation of which by IL-23 can provoke psoriasis-like inflammation^{1–4}. The skin is also innervated by a meshwork of peripheral nerves consisting of relatively sparse autonomic and abundant sensory fibres. Interactions between the autonomic nervous system and immune cells in lymphoid organs are known to contribute to systemic immunity, but how peripheral nerves regulate cutaneous immune responses remains unclear^{5,6}. We exposed the skin of mice to imiquimod, which induces IL-23-dependent psoriasis-like inflammation^{7,8}. Here we show that a subset of sensory neurons expressing the ion channels TRPV1 and Na_v1.8 is essential to drive this inflammatory response. Imaging of intact skin revealed that a large fraction of DDCs, the principal source of IL-23, is in close contact with these nociceptors. Upon selective pharmacological or genetic ablation of nociceptors^{9–11}, DDCs failed to produce IL-23 in imiquimod-exposed skin. Consequently, the local production of IL-23-dependent inflammatory cytokines by dermal $\gamma\delta$ T17 cells and the subsequent recruitment of inflammatory cells to the skin were markedly reduced. Intradermal injection of IL-23 bypassed the requirement for nociceptor communication with DDCs and restored the inflammatory response¹². These findings indicate that TRPV1⁺Na_v1.8⁺ nociceptors, by interacting with DDCs, regulate the IL-23/IL-17 pathway and control cutaneous immune responses.

Repeated topical application of imiquimod (IMQ) to murine skin provokes inflammatory lesions that resemble human psoriasis^{7,8}. This response is mediated by IL-23, which stimulates skin-resident $\gamma\delta$ T cells to secrete IL-17 and IL-22, cytokines that induce inflammatory leukocyte recruitment and acanthosis¹³. Indeed, antibodies targeting the shared p40 subunit of IL-12 and IL-23 inhibit both IMQ-induced murine dermatitis and human psoriasis^{8,13}. Frequent symptoms in human psoriasis, aside from the prominent skin lesions, include the sensations of itch, pain and discomfort in affected areas¹⁴. Clinical reports suggest that intralesionally administered anaesthetics or surgical denervation of psoriatic lesions not only abrogate local sensation, but also ameliorate local inflammation¹⁵. Similarly, in mutant mice with disseminated psoriasiform dermatitis, peripheral nerve dissection attenuated skin inflammation¹⁶; however, cutaneous nerves are composed of sympathetic and several types of sensory fibres, and the role of individual types of nerve fibres remains unclear⁶. Using the IMQ model, we investigated whether and how specific subsets of peripheral nerves contribute to the formation of psoriasiform skin lesions.

Skin sensations perceived as inflammatory pain, noxious heat and some forms of itch are transmitted by sensory fibres that express the cation channel TRPV1. Most TRPV1⁺ fibres co-express the sodium channel Na_v1.8 (refs 9–11). Na_v1.8⁺ nociceptors can be identified in the dermis of Na_v1.8-TdTomato (TdT) mice by their red fluorescence⁹ (Fig. 1a). Confocal microscopy of skin samples from Na_v1.8-TdT mice co-stained

for tyrosine hydroxylase (TH), which identifies sympathetic fibres, and for β 3-tubulin, a pan-neuronal marker, revealed that Na_v1.8⁺TH[−] nociceptors represent the vast majority of cutaneous nerve fibres, whereas Na_v1.8[−]TH⁺ sympathetic fibres are rare.

To investigate the roles of sympathetic fibres and nociceptors in the IMQ model, mice were treated systemically with either 6-hydroxydopamine (6OHDA) or reserpine (RTX) to ablate TH⁺ sympathetic neurons or TRPV1⁺ nociceptors, respectively^{11,17} (Extended Data Figs 1, 2). Subsequently, IMQ was applied topically to one ear and the ensuing inflammatory response was assessed based on the change in ear thickness, size of the myeloid infiltrate (Extended Data Fig. 3a) and tissue contents of inflammatory cytokines.

After sympathetic denervation, IMQ-induced ear swelling was reduced compared to controls (Extended Data Fig. 1c); however, the inflammatory infiltrate was increased, whereas IL-17A, IL-17F, IL-22 and IL-12/23p40 production remained unchanged (Extended Data Fig. 1d–i). Thus, sympathetic innervation exerts little or no direct local control over the inflammatory skin response. The observed changes were probably due to cardiovascular effects and/or global immune dysregulation after systemic sympathectomy⁵ (Supplementary Information). By contrast, in RTX-treated mice both ear swelling and inflammatory infiltrates in IMQ-exposed ears were profoundly reduced (Fig. 1b–e and Extended Data Fig. 4a–d). RTX treatment did not alter the systemic supply of inflammatory cells¹⁸ (Extended Data Fig. 4e, f). Moreover, intravital microscopy of ear skin revealed similar leukocyte rolling in RTX-treated and control mice (Extended Data Fig. 5), indicating that the absence of nociceptors did not affect the baseline adhesiveness of dermal microvessels¹⁹. It is more likely that ablation of TRPV1⁺ sensory nerves reduced IMQ-induced inflammation through local, extravascular mechanisms. However, the attenuated inflammatory response was not limited to the skin, as the IMQ-induced enhancement in cellularity of the draining auricular lymph node was also blunted by RTX (Fig. 1f).

Lymph nodes have a critical function in dermal antigen presentation to naive T cells and in the generation of migratory effector cells. They also possess peripheral innervation²⁰, which could have been altered by RTX; however, the role of skin-draining lymph nodes during psoriatic inflammation is unclear. To address this issue, we tested the effect of IMQ in lymphotoxin- α -deficient (LT α ^{−/−}) mice, which are devoid of lymph nodes. Compared with wild-type mice, there was no statistical difference in ear thickness, frequency or composition of the inflammatory infiltrate in ears of LT α ^{−/−} mice (Fig. 1g, h and data not shown). Additionally, we treated wild-type mice with FTY720, which blocks T-cell egress from lymph nodes, preventing trafficking of effector cells to peripheral tissues²¹. Again, IMQ elicited full-fledged inflammation in exposed ears (Fig. 1i, j and data not shown), indicating that T-cell priming in skin draining lymph nodes is dispensable for the acute induction of psoriasiform inflammation. Together, these findings imply that TRPV1⁺ nociceptors promote local immune responses directly in the skin.

Neutrophil recruitment to the skin and keratinocyte hyperproliferation, hallmarks of IMQ-induced inflammation, are driven by IL-17 and

¹Department of Microbiology and Immunobiology, Harvard Medical School, Boston, Massachusetts 02115, USA. ²Institute for Biomedical Research, University College London, London WC1E 6BT, UK.

*These authors contributed equally to this work.

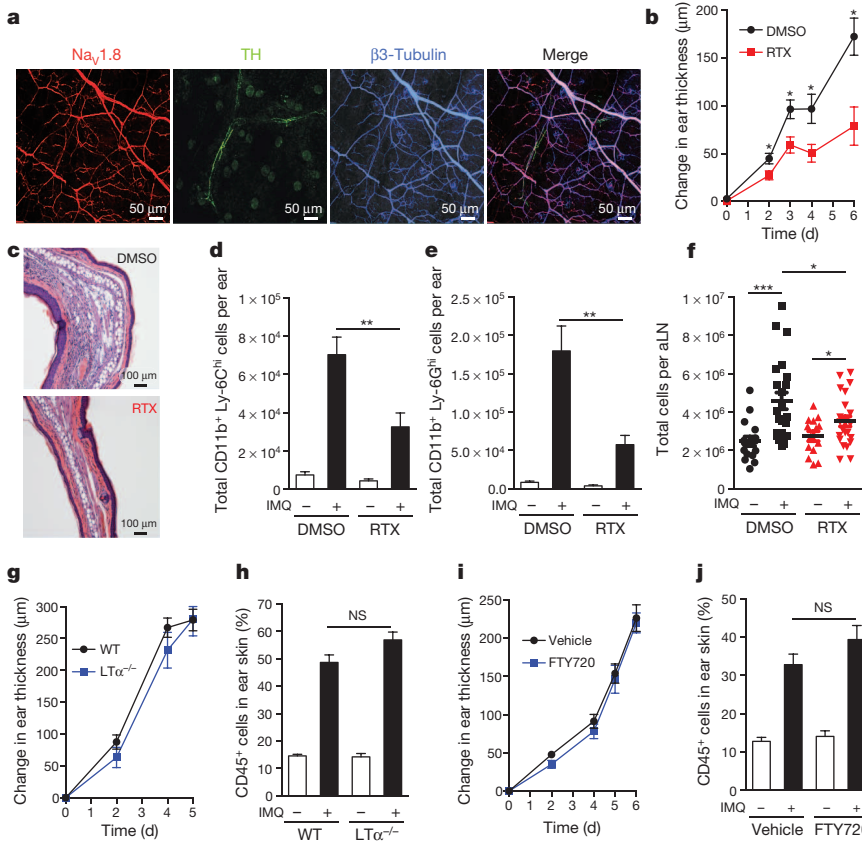
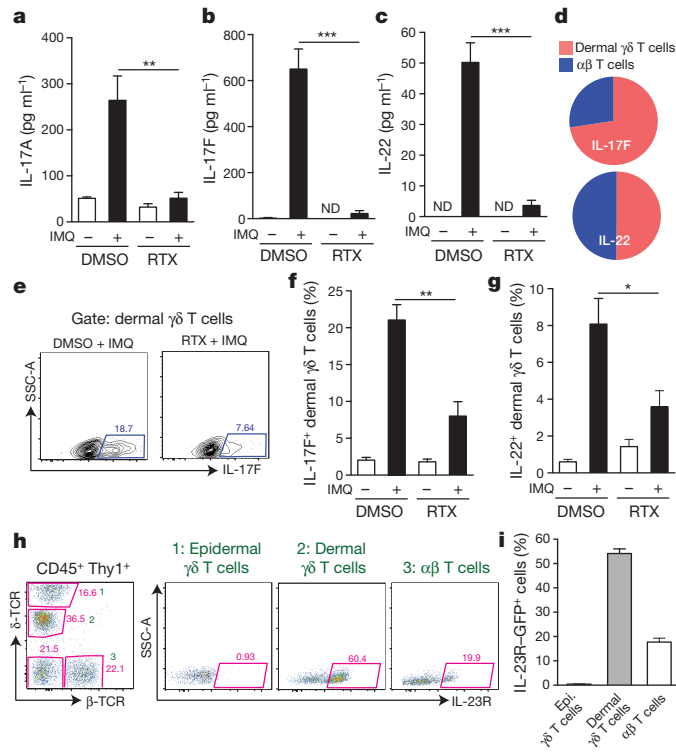


Figure 1 | TRPV1⁺ nociceptor ablation attenuates skin inflammation and draining lymph node hypertrophy in the IMQ model. **a**, Representative whole-mount confocal micrograph of normal ear skin from Na_v.1.8-TdT reporter mice (Na_v.1.8⁺ nociceptors, red) stained for TH (sympathetic nerves, green) and β3-tubulin (peripheral nerves, blue). **b–f**, The ear skin of vehicle (dimethylsulphoxide (DMSO))-treated controls or TRPV1⁺ nociceptor ablated (RTX) mice was treated with topical IMQ cream daily. **b**, Ear thickness was measured relative to the contralateral ear at indicated time points (*n* = 10–15 mice per time point; **P* < 0.02). **c**, Representative histological sections of IMQ-treated ears at day 6 stained by haematoxylin and eosin. **d, e**, Total inflammatory monocytes (*n* = 10) (**d**) and total neutrophils (**e**) in skin at day 3 (*n* = 10; ***P* < 0.005). **f**, Total cell number in auricular lymph nodes (aLNs) at day 3 (*n* = 20; **P* = 0.01; ****P* < 0.001). **g–j**, IMQ was applied daily to wild-type (WT; *n* = 10) and LTα^{-/-} mice (*n* = 6) (**g, h**) or vehicle-treated (*n* = 10) and FTY720-treated mice (*n* = 10) (**i, j**), and ear swelling was measured at the indicated time points (**g, i**). **h, j**, The percentage of CD45⁺ leukocytes was determined in ear skin digests on day 6. NS, not significant. Error bars show mean ± standard error of the mean (s.e.m.).

IL-22, respectively^{2,7,12}. We asked whether nociceptors regulate the production of these cytokines. Indeed, after IMQ treatment, protein levels of IL-17A, IL-17F and IL-22 had markedly increased in the ears of control mice, whereas in RTX-treated mice IL-17A was very low and IL-17F and IL-22 remained below the detection limit (Fig. 2a–c). Thus, TRPV1⁺ nociceptors control the generation of several key effector cytokines in psoriasisform dermatitis.



As our findings in FTY720-treated mice suggested that recruitment of lymph-node-derived effector T cells is not needed for IMQ-induced skin inflammation, we asked whether nociceptors regulate cytokine production by skin-resident lymphocytes, particularly γδT17 cells, which produce IL-17F and IL-22 (refs 3, 22, 23). In the ears of IMQ-treated control mice, most IL17F⁺ lymphocytes were dermal γδ T cells, whereas few conventional αβ T cells expressed IL-17F (Fig. 2d and Extended Data Figs 3b, 6a). In RTX-treated mice, both IL-17F⁺ and IL-22⁺ dermal γδ T cells were significantly reduced, indicating that TRPV1⁺ neurons drive the local production of IL-17F and IL-22 primarily by γδT17 cells (Fig. 2e–g and Extended Data Fig. 6b, c). These T cells seed the skin in early life and are poised for rapid IL-17 production upon stimulation by IL-23 (ref. 24). Indeed, in the ears of IL-23R^{GFP/+} mice²⁵, ~60% of dermal γδT17 and ~20% of αβ T cells expressed IL-23R (Fig. 2h, i), whereas T cells in auricular lymph nodes and epidermal γδ T cells expressed little or no IL-23R (Extended Data Fig. 6d, e).

In light of the preferential expression of IL-23R on dermal γδT17 cells, the known role of IL-23 as a driver of IL-17 and IL-22 generation in psoriasisform inflammation¹³ and our finding that RTX pre-treatment profoundly diminished IMQ-induced cytokine production by γδT17

Figure 2 | TRPV1⁺ nociceptors control IL-17F and IL-22 production by IL-23R⁺ dermal γδ T cells. **a–c**, After 3 days of IMQ challenge, ears from vehicle (DMSO)-treated mice (*n* = 5) or RTX-treated mice (*n* = 5) were harvested to perform enzyme-linked immunosorbent assays (ELISA) for IL-17A (**a**), IL-17F (**b**) and IL-22 (**c**). ***P* < 0.01, ****P* < 0.001. ND, not detected. **d–g**, Flow cytometry on digested ear skin was performed on day 6 of IMQ challenge. **d**, Relative frequency of IL-17F⁺ or IL-22⁺ dermal γδ T cells and αβ T cells in IMQ-treated control mice (*n* = 15). **e**, Representative FACS plots of IL-17F staining in dermal γδ T cells from vehicle (DMSO)- and RTX-treated mice. **f, g**, Quantification of frequency of IL-17F⁺ (**f**) and IL-22⁺ (**g**) among dermal γδ T cells in DMSO- and RTX-treated mice (*n* = 5 per group; **P* < 0.05; ***P* = 0.01). **h, i**, Representative FACS plots of normal ear skin from an IL-23R^{GFP/+} mouse (**h**) and quantification of frequency of IL-23R-GFP⁺ cells among skin-resident Thy1⁺ T-cell subsets (*n* = 8) (**i**). Epi., epidermal. Error bars show mean ± s.e.m.

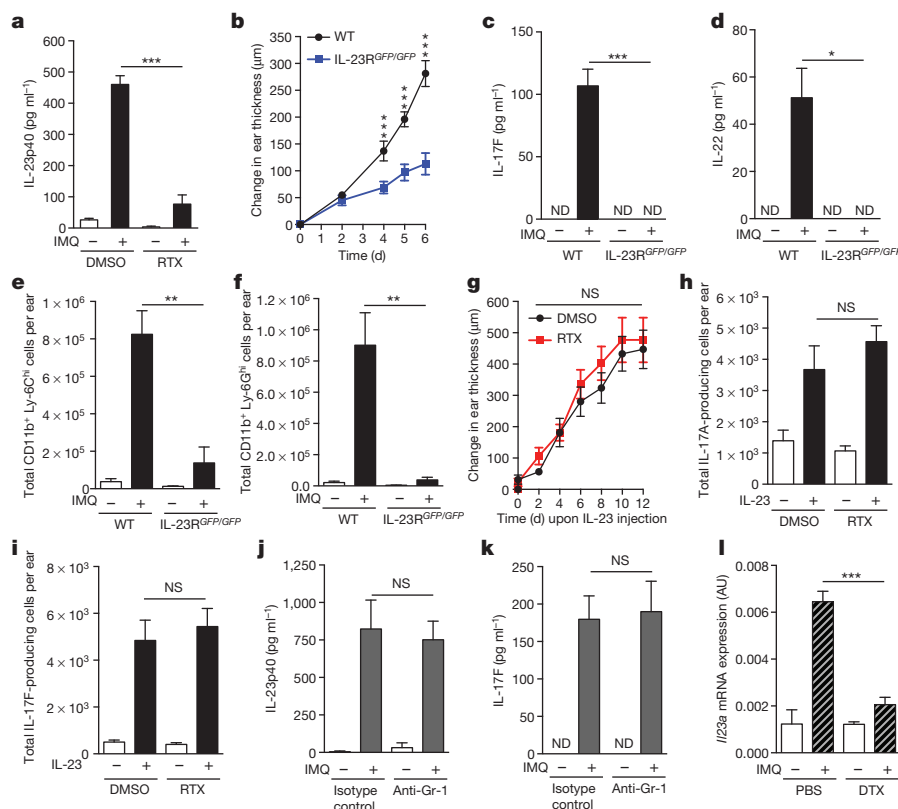
cells, we proposed that TRPV1⁺ nociceptors might control dermal IL-23 production. Topical IMQ treatment of control mice markedly increased p40 protein levels, as well as messenger RNA levels of *Il12b* (IL-12/23p40) and *Il23a* (IL-23p19), but not *Il12a* (IL-12p35). These effects were nearly abolished after RTX treatment (Fig. 3a and Extended Data Fig. 7a–c), suggesting that TRPV1⁺ nociceptors are essential for cutaneous IL-23 production. It seems unlikely that IL-12 had a major impact in the IMQ model, because IMQ-induced inflammatory parameters were considerably reduced in IL-23R^{GFP/GFP} mice, which respond to IL-12 but not IL-23 (Fig. 3b–f). However, IL-12-dependent skin inflammation induced using a chemical irritant, 2,4-dinitrofluorobenzene (DNFB)²⁶, was profoundly reduced in RTX-treated mice, suggesting that RTX-sensitive fibres also have a role in IL-12-driven dermatitis (Extended Data Fig. 7d, e).

Of note, although IL-17F and IL-22 production as well as myeloid infiltrates were virtually abolished in IL-23R^{GFP/GFP} mice, ear swelling was only partially reduced (Fig. 3b–f), suggesting that topical IMQ promotes modest tissue oedema through an IL-23-independent pathway. This activity was independent of nociceptors, as RTX treatment of IL-23R^{GFP/GFP} mice had no effect on the IMQ-induced swelling (Extended Data Fig. 7f).

Although the above findings clearly demonstrate that nociceptors are indispensable for IMQ-induced dermal IL-23 production, it remained possible that nociceptive fibres exert additional pro-inflammatory functions, for example, by directly regulating $\gamma\delta$ T17 cells. To address this, we

performed intradermal IL-23 injections, which trigger psoriasiform skin inflammation in murine skin¹². Regardless of whether nociceptors were ablated or left intact, IL-23 administration resulted in profound ear swelling and fully rescued IL-17A and IL-17F production by Thy1⁺ cells (Fig. 3h, i) and $\gamma\delta$ T17 cells (Extended Data Fig. 7g, h). Together, these results suggest that the pro-inflammatory function of TRPV1⁺ neurons is rooted exclusively in the promotion of IL-23 production, at least in this experimental setting.

Next, we sought to identify the IL-23-producing cell type(s) regulated by TRPV1⁺ nociceptors. In intestinal barrier tissues, Ly-6C^{high} inflammatory monocytes were identified as a major source of IL-23 in a colitis model²⁷. However, depletion of neutrophils and inflammatory monocytes with anti-Gr-1 did not affect IMQ-induced dermal IL-23p40 or IL-17F levels (Fig. 3j, k and Extended Data Fig. 8a), suggesting that skin-resident dendritic cells and/or macrophages rather than migratory myeloid cells were the critical source of IL-23. Thus, we injected CD11c-diphtheria toxin receptor (DTR) mice with diphtheria toxin (DTX), which depleted DDCs and Langerhans cells, but not macrophages (Extended Data Fig. 8b, c). After DTX treatment, IMQ-induced expression of *Il23a* mRNA was markedly reduced in treated ears (Fig. 3l). Although these results do not discriminate between the relative contributions of Langerhans cells and DDCs to IL-23 production, IL-34-deficient mice—which selectively lack Langerhans cells—are not impaired in IMQ-induced skin inflammation⁸. We focused our analysis on DDCs, which can be



of DMSO- or RTX-treated mice ($n = 8$ per group). **g**, Ear thickness was measured as indicated. **h, i**, After 3 days, the number of IL-17A-producing (**h**) and IL-17F-producing (**i**) Thy1⁺ cells per ear was quantified by FACS ($n = 5$). **j, k**, Mice were treated with anti-Gr-1 to deplete neutrophils and inflammatory monocytes or isotype-matched control monoclonal antibody and challenged with IMQ for 3 days. Ear skin protein lysates were analysed for IL-23p40 (**j**) and IL-17F (**k**) by ELISA ($n = 5$). **l**, CD11c-DTR mice were treated with DTX or PBS 12 h before IMQ challenge. After 6 h, ears were harvested and processed for total RNA isolation and *Il23a* mRNA levels were analysed by quantitative polymerase chain reaction (qPCR) ($n = 4$; $***P = 0.001$). AU, arbitrary units. ND, not detected; NS, not significant. Error bars show mean \pm s.e.m.

of DMSO- or RTX-treated mice ($n = 8$ per group). **g**, Ear thickness was measured as indicated. **h, i**, After 3 days, the number of IL-17A-producing (**h**) and IL-17F-producing (**i**) Thy1⁺ cells per ear was quantified by FACS ($n = 5$). **j, k**, Mice were treated with anti-Gr-1 to deplete neutrophils and inflammatory monocytes or isotype-matched control monoclonal antibody and challenged with IMQ for 3 days. Ear skin protein lysates were analysed for IL-23p40 (**j**) and IL-17F (**k**) by ELISA ($n = 5$). **l**, CD11c-DTR mice were treated with DTX or PBS 12 h before IMQ challenge. After 6 h, ears were harvested and processed for total RNA isolation and *Il23a* mRNA levels were analysed by quantitative polymerase chain reaction (qPCR) ($n = 4$; $***P = 0.001$). AU, arbitrary units. ND, not detected; NS, not significant. Error bars show mean \pm s.e.m.

further subdivided into CD103⁺ and CD11b⁺ subsets²⁸. Both subsets, as well as macrophages, were sorted by fluorescence-activated cell sorting (FACS) from IMQ-treated and control ears to measure mRNA for *Il23a* and *Il12a*. Although CD103⁺ DDCs showed the most notable upregulation of *Il23a* mRNA, taking into consideration that CD11b⁺ DDCs are more abundant, we estimate that the latter subset produced ~75% of the *Il23a* mRNA, consistent with a recent report²⁹ (Fig. 4a and Extended Data Fig. 8c, d).

Having identified DDCs as the principal source of IMQ-induced IL-23, we sought to characterize the spatial relationship between DDCs and cutaneous nerves. Remarkably, confocal microscopy of skin whole mounts revealed that at steady state ~75% of DDCs were either in direct contact or in close proximity to sensory nerves (Fig. 4b–d and Extended Data Fig. 9a). Interactions were apparent along the entire length of nerves, suggesting that DDCs may receive signals from unmyelinated nociceptor axons and not just from nerve terminals. However, given the high density of peripheral nerves in the skin, it was difficult to judge whether the association with DDCs occurred merely by chance or reflected a biased distribution. To address this possibility, we compared DDC localization relative to two other dense anatomical structures: blood and lymph vessels. In resting tissues, contacts of DDCs with these microvascular networks were only about half as frequent as with peripheral nerves (Fig. 4d).

Of note, even though inflammation enhances DDC motility and egress into draining lymphatics, IMQ challenge did not alter the frequency of DDCs contacting nerves (Extended Data Fig. 9b), suggesting that DDCs engaged in dynamic interactions with nociceptors. We reconstituted Na_v1.8-TdT mice with yellow fluorescent protein (YFP)-tagged CD11c bone marrow and performed time-lapse multiphoton-intravital microscopy (MP-IVM) in ear skin to generate three-dimensional time-lapse videos of interactions between YFP⁺ DDCs and TdT⁺ nociceptors. These interactions were highly diverse (Supplementary Video 1); some DDCs seemed to be anchored on nerves and sometimes extended protrusions to probe the surrounding tissue, whereas others appeared to use nerve fibres as a scaffold for directional migration (Supplementary Video 2).

Together, our results support the idea that DDCs can physically interact with a subset of nociceptors that regulate the production of IL-23. However, it should be cautioned that the pharmacological target of RTX, TRPV1, is also expressed on some non-neuronal cells¹⁰. Consequently,

we sought an alternative to confirm the role of nociceptors in an experimental system that does not rely on pharmacologically targeting TRPV1. To this end, we used Na_v1.8-diphtheria toxin (DTA) mice in which Na_v1.8⁺ fibres, which respond to mechanical pressure, inflammatory pain and noxious cold, are selectively deleted⁹. Although nociceptor-associated transcripts in dorsal root ganglia were more profoundly reduced in this genetic model than after RTX treatment, *Trpv1* mRNA levels were only reduced by ~80%, consistent with the fact that noxious heat sensing fibres express TRPV1, but not Na_v1.8 (Extended Data Figs 2c, 9c)⁹. After IMQ challenge, the ears of Na_v1.8-DTA mice contained very low protein levels of IL-17A, IL-17F, IL-22 and IL-23p40 as compared to littermate controls (Fig. 4e–h). We conclude that Na_v1.8⁺ TRPV1⁺ neurons are insufficient to induce IL-23 production; rather, Na_v1.8⁺ TRPV1⁺ nociceptors are driving the response.

In light of these results, we propose a model of cutaneous neuroimmune interactions (Extended Data Fig. 10) whereby dermal Na_v1.8⁺ TRPV1⁺ nociceptors are essential to induce IL-23 production by nearby DDCs. IL-23 then acts on IL-23R⁺ γδT17 cells to induce IL-17F and IL-22 secretion, which precipitates the recruitment of circulating neutrophils and monocytes driving psoriasiform skin inflammation. The fact that both RTX and Na_v1.8-DTA mice largely preserve a dense meshwork of dermal nerves (Extended Data Fig. 9d, e) implies that DDCs do not simply rely on nerves as a scaffold from which to produce IL-23. It is more likely that Na_v1.8⁺ TRPV1⁺ nociceptors actively induce and control IL-23 production.

Although further studies will be needed to determine the precise molecular underpinnings of neuroimmune communication in the skin (Supplementary Information), the present findings indicating nociceptor-mediated control of DDCs and the IL-23/IL-17 axis open new avenues for the treatment of inflammatory diseases in the skin and perhaps elsewhere. Intriguingly, recent work has shown that Na_v1.8⁺ nerve fibres exert immunosuppressive activity during *Staphylococcus aureus* infection³⁰, raising the possibility that some pathogens have evolved mechanisms to subvert the pro-inflammatory function of nociceptors. Together, this recent work and the present study suggest an emerging new paradigm whereby TRPV1⁺ Na_v1.8⁺ nociceptive fibres integrate environmental signals to modulate local immune responses to a variety of infectious and inflammatory stimuli.

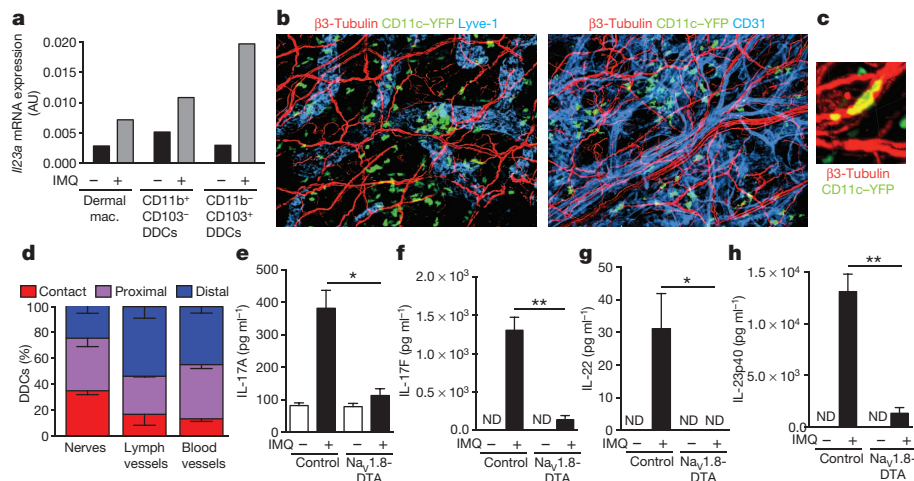


Figure 4 | DDCs are closely associated with cutaneous nerves and depend on Na_v1.8⁺ nociceptors for IMQ-induced IL-23 production.

a, Mice were challenged with IMQ ($n = 20$ pooled mice per condition) and, after 6 h, myeloid cell populations comprising dermal macrophages (mac.) and two subsets of DDCs were FACS sorted (Extended Data Fig. 8c) from cell suspensions to measure *Il23a* mRNA by qPCR. **b**, Representative confocal micrographs of ear skin whole mounts from CD11c-YFP mice stained for $\beta 3$ -tubulin (peripheral nerves, red) and Lyve-1 (lymphatics, blue) or CD31 (blood and lymphatic endothelial cells, blue). Original magnification, $\times 200$. **c**, Close-up confocal micrograph of a CD11c-YFP cell in contact with

a nerve (see also Supplementary Videos 1, 2). **d**, Quantification of three-dimensional DDC proximity to peripheral nerves, lymphatics and blood vessels in normal ear skin. The frequency of DDCs ($n = 330$) in contact, proximal (0–7 μm) and distal ($>7 \mu\text{m}$) to nerve fibres was determined as described in Methods and a Chi-squared test showed bias of DDCs to nerves relative to lymphatics and blood vessels ($**P < 0.0001$). **e–h**, Ears of Na_v1.8-DTA or control littermates were treated daily with IMQ. Total protein was prepared from ear skin after 3 days and IL-17A (**e**), IL-17F (**f**), IL-22 (**g**) and IL-23p40 (**h**) were quantified by ELISA ($n = 4$ ears per condition; $*P < 0.05$; $**P < 0.01$). ND, not detected. Error bars show mean \pm s.e.m.

METHODS SUMMARY

Published mouse strains used in this study are detailed in Methods. $\text{Na}_v1.8\text{-Cre mice}^9$ were bred with Rosa26-DTA and Rosa26-TdT mice to generate $\text{Na}_v1.8\text{-DTA mice}$ for functional studies and $\text{Na}_v1.8\text{-TdT mice}$ for imaging, respectively. TRPV1⁺ nociceptors were deleted using three escalating doses ($30 \mu\text{g kg}^{-1}$, $70 \mu\text{g kg}^{-1}$ and $100 \mu\text{g kg}^{-1}$) of RTX as described previously¹¹. To induce psoriasisform ear inflammation, 8–12-week-old mice were treated topically with 5% IMQ cream or injected with 500 ng per ear recombinant (r)IL-23. Ear thickness was measured using an engineer's micrometer (Mitutoyo). Cytokines were quantified from skin protein extracts by ELISA (Biolegend, R&D). For flow cytometric analysis of tissue leukocyte markers and intracellular cytokines, single-cell suspensions from ear skin were prepared by enzymatic digestion⁴. Imaging of fixed skin tissue was performed using an Olympus Fluoview BX50WI inverted microscope, and MP-IVM in live anaesthetized mice was performed using an upright microscope (Prairie Technologies) with a MaiTai Ti:sapphire laser (Spectra-Physics). All animal studies were approved by the Institutional Animal Care and Use Committee of Harvard Medical School and complied with National Institutes of Health guidelines.

Online Content Any additional Methods, Extended Data display items and Source Data are available in the online version of the paper; references unique to these sections appear only in the online paper.

Received 27 August 2013; accepted 4 March 2014.

Published online 23 April 2014.

- Nestle, F. O., Di Meglio, P., Qin, J. Z. & Nickoloff, B. J. Skin immune sentinels in health and disease. *Nature Rev. Immunol.* **9**, 679–691 (2009).
- Perera, G. K., Di Meglio, P. & Nestle, F. O. Psoriasis. *Annu. Rev. Pathol.* **7**, 385–422 (2012).
- Cai, Y. *et al.* Pivotal role of dermal IL-17-producing $\gamma\delta$ T cells in skin inflammation. *Immunity* **35**, 596–610 (2011).
- Gray, E. E., Suzuki, K. & Cyster, J. G. Cutting edge: identification of a motile IL-17-producing $\gamma\delta$ T cell population in the dermis. *J. Immunol.* **186**, 6091–6095 (2011).
- Rosas-Ballina, M. *et al.* Acetylcholine-synthesizing T cells relay neural signals in a vagus nerve circuit. *Science* **334**, 98–101 (2011).
- Chiu, I. M., von Hehn, C. A. & Woolf, C. J. Neurogenic inflammation and the peripheral nervous system in host defense and immunopathology. *Nature Neurosci.* **15**, 1063–1067 (2012).
- van der Fits, L. *et al.* Imiquimod-induced psoriasis-like skin inflammation in mice is mediated via the IL-23/IL-17 axis. *J. Immunol.* **182**, 5836–5845 (2009).
- Flutter, B. & Nestle, F. O. TLRs to cytokines: mechanistic insights from the imiquimod mouse model of psoriasis. *Eur. J. Immunol.* **43**, 3138–3146 (2013).
- Abrahamsen, B. *et al.* The cell and molecular basis of mechanical, cold, and inflammatory pain. *Science* **321**, 702–705 (2008).
- Lumpkin, E. A. & Caterina, M. J. Mechanisms of sensory transduction in the skin. *Nature* **445**, 858–865 (2007).
- Sándor, K., Helyes, Z., Elekes, K. & Szolcsanyi, J. Involvement of capsaicin-sensitive afferents and the transient receptor potential vanilloid 1 receptor in xylene-induced nocifensive behaviour and inflammation in the mouse. *Neurosci. Lett.* **451**, 204–207 (2009).
- Zheng, Y. *et al.* Interleukin-22, a T_H17 cytokine, mediates IL-23-induced dermal inflammation and acanthosis. *Nature* **445**, 648–651 (2007).
- Lowes, M. A., Russell, C. B., Martin, D. A., Towne, J. E. & Krueger, J. G. The IL-23/17 pathogenic axis in psoriasis is amplified by keratinocyte responses. *Trends Immunol.* **34**, 174–181 (2013).
- Rapp, S. R., Feldman, S. R., Exum, M. L., Fleischer, A. B. Jr & Reboussin, D. M. Psoriasis causes as much disability as other major medical diseases. *J. Am. Acad. Dermatol.* **41**, 401–407 (1999).
- Farber, E. M., Lanigan, S. W. & Boer, J. The role of cutaneous sensory nerves in the maintenance of psoriasis. *Int. J. Dermatol.* **29**, 418–420 (1990).
- Ostrowski, S. M., Belkadi, A., Loyd, C. M., Diaconu, D. & Ward, N. L. Cutaneous denervation of psoriasisform mouse skin improves acanthosis and inflammation in a sensory neuropeptide-dependent manner. *J. Invest. Dermatol.* **131**, 1530–1538 (2011).
- Grebe, K. M. *et al.* Sympathetic nervous system control of anti-influenza CD8⁺ T cell responses. *Proc. Natl Acad. Sci. USA* **106**, 5300–5305 (2009).
- Swirski, F. K. *et al.* Identification of splenic reservoir monocytes and their deployment to inflammatory sites. *Science* **325**, 612–616 (2009).
- Weninger, W. *et al.* Specialized contributions by $\alpha(1,3)$ -fucosyltransferase-IV and FucT-VII during leukocyte rolling in dermal microvessels. *Immunity* **12**, 665–676 (2000).
- Iannacone, M. *et al.* Subcapsular sinus macrophages prevent CNS invasion on peripheral infection with a neurotropic virus. *Nature* **465**, 1079–1083 (2010).
- Matloubian, M. *et al.* Lymphocyte egress from thymus and peripheral lymphoid organs is dependent on S1P receptor 1. *Nature* **427**, 355–360 (2004).
- Gray, E. E. *et al.* Deficiency in IL-17-committed $\text{V}_\beta4^+ \gamma\delta$ T cells in a spontaneous Sox13-mutant CD45.1⁺ congenic mouse substrain provides protection from dermatitis. *Nature Immunol.* **14**, 584–592 (2013).
- Pantelyushin, S. *et al.* Ror γ ⁺ innate lymphocytes and $\gamma\delta$ T cells initiate psoriasisform plaque formation in mice. *J. Clin. Invest.* **122**, 2252–2256 (2012).
- Guo, L., Junttila, I. S. & Paul, W. E. Cytokine-induced cytokine production by conventional and innate lymphoid cells. *Trends Immunol.* **33**, 598–606 (2012).
- Awasthi, A. *et al.* Cutting edge: IL-23 receptor GFP reporter mice reveal distinct populations of IL-17-producing cells. *J. Immunol.* **182**, 5904–5908 (2009).
- Muller, G. *et al.* IL-12 as mediator and adjuvant for the induction of contact sensitivity *in vivo*. *J. Immunol.* **155**, 4661–4668 (1995).
- Zigmond, E. *et al.* Ly6C^{hi} monocytes in the inflamed colon give rise to proinflammatory effector cells and migratory antigen-presenting cells. *Immunity* **37**, 1076–1090 (2012).
- Guilliams, M. *et al.* From skin dendritic cells to a simplified classification of human and mouse dendritic cell subsets. *Eur. J. Immunol.* **40**, 2089–2094 (2010).
- Wohn, C. *et al.* Langerin^{neg} conventional dendritic cells produce IL-23 to drive psoriatic plaque formation in mice. *Proc. Natl Acad. Sci. USA* **110**, 10723–10728 (2013).
- Chiu, I. M. *et al.* Bacteria activate sensory neurons that modulate pain and inflammation. *Nature* (2013).

Supplementary Information is available in the online version of the paper.

Acknowledgements We thank G. Cheng, M. Flynn and S. Omid for technical support; M. Perdue, L. Jones and E. Nigro for secretarial assistance; E. Gray for providing detailed protocols for flow cytometry of skin samples; J. Harris for discussion and providing detailed RNA isolation protocols of skin samples; R. T. Roderick for histopathology analysis; T. Liu and J. Ru-Rong for providing the RTX denervation protocol; M. Ghebremichael for statistical advice; F. Winau and J. L. Rodriguez-Fernandez for critical reading of the manuscript and members of the von Andrian laboratory for discussion and advice. This work was supported by National Institutes of Health (NIH) grants AI069259, AI078897, AI095261 and AI111595 (to U.H.v.A.), NIH 5F31AR063546-02 (to J.O.-M.) and the Human Frontiers Science Program, Charles A. King Trust and National Psoriasis Foundation (to L.R.-B.).

Author Contributions L.R.-B., J.O.-M., and U.H.v.A. designed the study. L.R.-B., J.O.-M., M.P., E.N., A.T. and D.A. performed and collected data from experiments, and L.R.-B., J.O.-M., A.T. and E.N. analysed data. J.N.W. provided reagents and gave conceptual advice. J.O.-M., L.R.-B. and U.H.v.A. wrote the manuscript.

Author Information Reprints and permissions information is available at www.nature.com/reprints. The authors declare no competing financial interests. Readers are welcome to comment on the online version of the paper. Correspondence and requests for materials should be addressed to U.H.v.A. (uva@hms.harvard.edu).

METHODS

Mice. C57BL/6 mice, 4–8 weeks old, were purchased from Charles River or the Jackson Laboratory and female mice were used in experiments. IL-23R^{GFP/GFP} mice²⁵, in which GFP is knocked into the cytoplasmic tail of IL-23R and the homozygous GFP mouse acts as a functional receptor knockout, were provided by M. Oukka and both male and female mice were used in experiments. CD11c-YFP mice³¹ were a gift from M. Nussenzweig and both male and female mice were used in experiments. LT $\alpha^{-/-}$ mice³² were purchased from the Jackson Laboratory and male mice were used in experiments. CD11c-DTR³³ mice were purchased from Jackson Laboratory and both male and female mice were used in experiments. Na_v1.8-Cre mice were previously described⁹. Rosa26-DTA mice and Rosa26-TdT mice, which express a floxed-STOP cassette upstream of the ubiquitously expressed Rosa26-DTA or Rosa26-TdT construct, respectively, were purchased from Jackson Laboratory. Na_v1.8-Cre male mice were bred with Rosa26-DTA and Rosa26-TdT female mice to generate Na_v1.8-DTA for functional studies and Na_v1.8-TdT for imaging experiments, respectively, of which both matched male and female litters were used in experiments. Glial fibrillary acidic protein (GFAP)-TdT mice were generated by crossing heterozygous GFAP-Cre mice³⁴ purchased from Jackson Laboratory with Rosa26-TdT mice. MHC-II-GFP mice³⁵ were provided by M. Boes. Bone marrow chimaeras were generated by irradiating Na_v1.8-TdT mice or GFAP-TdT mice with two split doses totalling 1,300 rad and reconstituting with CD11c-YFP or MHC-II-GFP unfractionated bone marrow injected intravenously, respectively. Bone marrow chimaeras were allowed to rest for 12 weeks before use. Mice were all housed in specific pathogen-free conditions in accordance with the National Institutes of Health and all experimental animal protocols were approved by the Institutional Animal Care and Use Committee at Harvard Medical School. For most animal experiments, because the contralateral ear served as a control for the ear in which an inflammatory stimulus was applied, no randomization was used. Investigators were blinded for the initial ear-swelling experiments and subsequently no blinding was used.

Denervation. RTX, a capsaicin analogue, was injected subcutaneously into the flank of 4-week-old mice in three escalating (30 $\mu\text{g kg}^{-1}$, 70 $\mu\text{g kg}^{-1}$ and 100 $\mu\text{g kg}^{-1}$) doses on consecutive days¹¹. Control mice were treated with vehicle solution (DMSO in PBS). Mice were allowed to rest for 4 weeks before denervation was confirmed by tail-flick assay. The tail-flick assay was conducted by holding mice vertically in a relaxed fashion allowing their tail to be immersed in a temperature-controlled water bath maintained at 52 °C. Denervated mice exhibited a tail-flick latency of >10 s. Besides insensitivity to noxious heat stimuli, overall behaviour qualitatively remained unaltered in RTX-treated mice. For chemical sympathectomy, mice were intraperitoneally injected with 80 mg kg^{-1} 6-OHDA in 0.01% ascorbic acid in PBS at day -3. Control mice received injections of 0.01% ascorbic acid in PBS¹⁷.

IMQ and DNFB treatment, IL-23 injection and ear measurement. Mice, 8–12 weeks old, of indicated genotypes or pharmacological treatments, were treated with 25 mg of 5% IMQ applied topically to dorsal and ventral aspects of ear skin totalling 1,250 μg of IMQ per day. Mice were treated starting on day 0 three times and killed for analyses on day 3 or were treated six times and killed for analyses on day 6. IL-23 was injected intradermally into the dorsal aspect of the ear skin as a 50 $\mu\text{g ml}^{-1}$ solution in 10 μl PBS (500 ng per ear). Contralateral ears were injected with PBS alone. A 0.5% solution of DNFB in acetone was applied to the dorsal and ventral aspects of ear skin without prior sensitization. Ear thickness was measured using an engineer's micrometer (Mitutoyo) at the indicated time points and the change in ear thickness is calculated as the change in ear thickness from the treated ear relative to the contralateral naive or vehicle-treated ear.

FTY720 treatment and depletion of myeloid cells. FTY720 (1 mg kg^{-1}), an agonist which results in S1P receptor internalization, or PBS was injected daily intraperitoneally starting from day 0 of IMQ challenge. Efficacy of treatment was confirmed by a marked reduction in circulating lymphocytes from peripheral blood (data not shown). To deplete dendritic cells from skin, CD11c-DTR mice³³ were injected at day -1 with 4 ng of DTX per g mouse, a dose that is nontoxic to murine cells not expressing the DTR³⁶. Depletion of DDCs and Langerhans cells, but not macrophages, was confirmed by flow cytometry (Extended Data Fig. 8). To deplete neutrophils and inflammatory monocytes, 500 μg of anti-Gr-1 per mouse (clone RB6-8C5; BioXCell), was injected intraperitoneally at days -1, 0, 1 and 2. Depletion was confirmed by flow cytometry of peripheral blood as well as challenged ear skin showing a paucity of neutrophils and inflammatory monocytes (Extended Data Fig. 8).

Histology. Ears were embedded in paraffin and submitted for histological analysis by haematoxylin and eosin staining to the Harvard Rodent Histopathology Core.

Whole-mount immunofluorescence of ear skin. Ears were harvested and split into dorsal and ventral halves. After fixation in 4% paraformaldehyde, any adherent cartilage was removed under a dissecting microscope to expose the dermis evenly for imaging. Tissue was blocked in blocking buffer containing PBS with 0.5% BSA, 0.3% Triton X-100, 10% goat serum and Fc Block and also stained with the following antibodies in the same buffer. Unconjugated antibodies used include: anti-neuronal

class III β -tubulin (clone TUJ1; Covance), anti-TH (clone A2B5-105; Millipore), anti-Lyve-1 (clone ALY7; eBiosciences), anti-peripherin (Polyclonal; Abcam) and anti-NeuN (A60; Millipore). Alexa488-conjugated antibodies include: anti-neuronal class III β -tubulin (clone TUJ1; Covance), goat anti-mouse IgG (Invitrogen) and goat anti-rabbit IgG. Alexa647-conjugated antibodies include: goat anti-rat IgG and goat anti-rabbit IgG. Washing steps were performed in PBS with 0.2% BSA, and 0.1% Triton X-100. Ears were mounted with the dermis facing the imaging plane in FluorSave reagent (Calbiochem).

Confocal microscopy. Confocal images were acquired on an Olympus Fluoview BX50WI inverted microscope with $\times 10/0.4$, $\times 20/0.5$ and $\times 40/1.3$ magnification/numerical aperture objectives. For images used in three-dimensional analysis, image planes were acquired at 0.5 μm intervals through the imaging volume.

Intravital two-photon microscopy. Anaesthetized mice were placed on a custom-built stage and the ear was fixed to a temperature-controlled metallic support to facilitate exposure of the dorsal aspect to the water-immersion $\times 20$ objective (0.95 numerical aperture) of an upright microscope (Prairie Technologies). A MaiTai Ti:sapphire laser (Spectra-Physics) was tuned between 870 nm and 900 nm for multiphoton excitation and second-harmonic generation. For dynamic analysis of cell interaction in four dimensions, several x - y sections (512 \times 512) with z spacing ranging from 2 μm to 4 μm were acquired every 15–20 s with an electronic zoom varying from 1 \times to 3 \times . Emitted light and second-harmonic signals were directed through 450/80 nm, 525/50 nm and 630/120 nm bandpass filters and detected with non-descanned detectors. Post-acquisition image analysis, volume rendering and four-dimensional time-lapse videos were performed using Imaris software (Bitplane scientific software).

Intravital microscopy and image analysis. Intravital microscopy of skin was performed as previously described¹⁹. In brief, control or RTX-treated mice were anaesthetized and the left ear was exposed and positioned for epifluorescence intravital microscopy. Preparations were transferred to an intravital microscope (IV-500; Mikron Instruments), equipped with a Rapp OptoElectronic SP-20 xenon flash lamp system and QImaging Rolera-MGi EMCCD camera. The fluorescent dye rhodamine-6G (20 mg kg^{-1} in PBS) was administered through the catheterized right carotid artery to visualize circulating leukocytes. Cell behaviour in skin venules was recorded in 10 min recordings through $\times 10$ or $\times 20$ water-immersion objectives (Achromplan; Carl Zeiss). Rolling fractions in individual vessel segments were determined offline by playback of digital video files. The rolling fraction was determined as the percentage of cells interacting with skin venules in the total number of cells passing through a vessel during the observation period.

Cytokine quantification by ELISA. Skin biopsies from ears were obtained using 10 mm diameter skin biopsy punches (Acuderm). Samples were homogenized in Tissue Extraction Reagent I (Invitrogen) in the presence of protease inhibitor cocktail (Roche) using a gentleMACS dissociator (Miltenyi Biotec). Skin protein extracts were assayed for IL-17A, IL-22, IL-23p40 (Biolegend) and IL-17F (R&D Systems) in accordance with the manufacturer's instructions.

RNA isolation and qPCR. RNA from sorted and pelleted cells was isolated using RNeasy Plus Mini Kit (Qiagen) including a gDNA elimination step. Ear skin and dorsal root ganglia (DRGs) were harvested and placed immediately in RNALater (Ambion) before homogenization and RNA isolation using Qiagen RNeasy Plus Mini Kit (Qiagen)⁹. DRGs for comparison of the efficacy of denervation were harvested from equivalent anatomical locations, typically consisting of the cervical and thoracic ganglia from C1–T2. cDNA synthesis was done using Superscript Vilo cDNA synthesis kit (Invitrogen) following the manufacturer's instructions. Relative quantification of transcripts was done using validated Quantitect Primer Assays (Qiagen) combined with the QuantiTect SYBR Green Detection Kit (Qiagen) on a LightCycler 480 (Roche). Relative expression of genes was calculated to *Gapdh* using the $\Delta\Delta\text{C}_\text{T}$ method.

Tissue digestion. Single-cell suspensions of lymph nodes, spleen and bone marrow were generated as described previously²⁰. For ear skin digestion, the dorsal and ventral aspects of the ear were mechanically separated before mincing and placing into a digestion mix modified from that described previously⁴. Ears were digested for 80 min at 37 °C in gentleMACS tubes (Miltenyi) with gentle agitation in freshly prepared digestion mix consisting of DMEM (Gibco) supplemented with HEPES (Invitrogen), 2% FCS, 100 $\mu\text{g ml}^{-1}$ Liberase TM (Roche), 100 $\mu\text{g ml}^{-1}$ DNase I (Roche) and 0.5 mg ml^{-1} Hyaluronidase (Sigma). After enzymatic digestion, the mixture was processed using a gentleMACS homogenizer (Miltenyi) to obtain a cell suspension, which was then filtered through a 70 μm cell strainer (BD). Cells were then resuspended in FACS buffer for analysis. If cell suspensions were to be analysed for cytokine-producing cells, ears were harvested and digested in the presence of Brefeldin A (Biolegend).

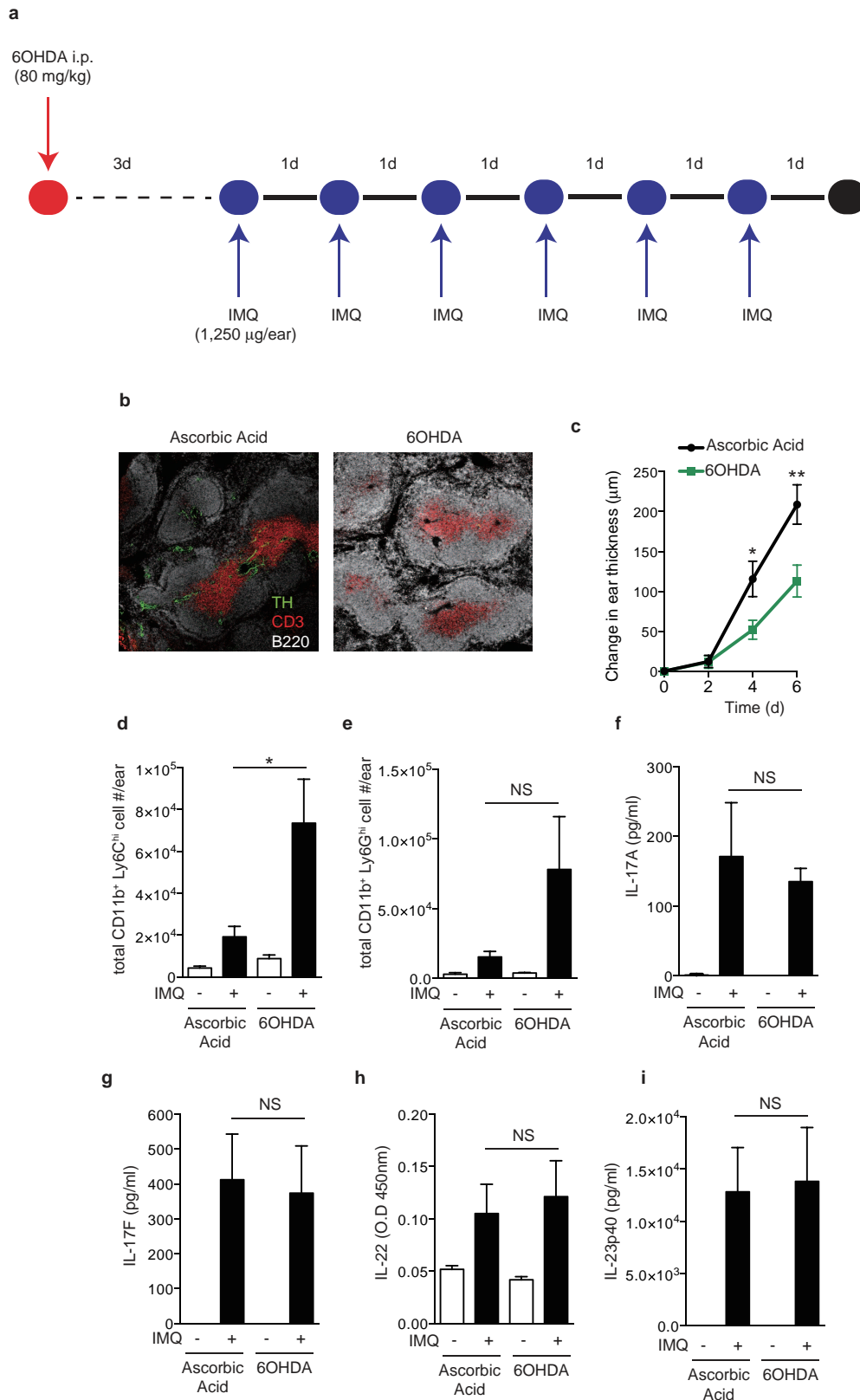
Flow cytometry, cell sorting and cell counts. Single-cell suspensions in FACS Buffer (PBS with 2 mM EDTA and 2% FCS (Invitrogen-GIBCO)) were pre-incubated with Fc Block (clone 2.4G2) before staining for surface antigens. FITC-conjugated antibodies used include: anti-Ly-6G (clone 1A8; BD Pharmingen). Alexa488-conjugated

antibodies used include: anti-CD103 (clone 2E7; Biolegend). PE-conjugated antibodies used include: anti- δ -TCR (clone GL3; Biolegend), anti-Ly-6C (clone HK1.4; Biolegend). PerCP/Cy5.5-conjugated antibodies used include: anti-CD45.2 (clone 104; Biolegend). PE-Cy7-conjugated antibodies include: anti-TCR- β (clone H57-597; Biolegend), anti-CD11c (clone HL3; BD Pharmingen). Alexa647-conjugated antibodies used include: anti-CCR6 (clone 140706; BD Pharmingen), anti-CD11b (clone M1/70; Biolegend). APC-Cy7-conjugated antibodies used include: anti-Thy1.2/CD90.2 (clone 30-H12; Biolegend), anti-I-A/I-E 'Class-II' (clone M5/114.15.2; Biolegend). Cells were then washed with PBS and resuspended in MACS buffer for immediate acquisition or fixed in Cytotfix (BD Pharmingen) as per the manufacturer's instructions for later acquisition. For analysis, cells were acquired on a BD FACS CANTO (BD Pharmingen) and analysed using FlowJo software (Treestar). For intracellular cytokine staining, cells were not restimulated and rather harvested and digested in the presence of Brefeldin A (Biolegend). After staining for surface antigens, cells were then fixed and permeabilized using BD Cytotfix/Cytoperm kit (BD Pharmingen) as per the manufacturer's instructions. Cells were stained in Perm/Wash buffer. Alexa488-conjugated antibodies used include: anti-IL-17A (clone TC11-18H10.1; Biolegend), anti-IL-17F (clone 9D3.1C8; Biolegend). Alexa647-conjugated antibodies used include: anti-IL-17A (clone TC11-18H10.1; Biolegend), anti-IL-17F (clone 9D3.1C8; Biolegend) and anti-IL-22 (clone Poly5164; Biolegend). For determining total counts of cell subsets, an aliquot of the same cell suspension used for flow cytometry was stained for CD45.2 and acquired on an Accuri Cytometer (BD Biosciences) with a known amount of CountBright counting beads (Invitrogen). The total CD45⁺ cell number was then determined in the original cell suspension and used for total quantification of the cell number of each subset of interest defined by multi-parameter flow cytometry based on that subset's frequency relative to the CD45⁺ population. For cell sorting, cells were stained for indicated surface markers and sorted using a BD FACSAria (BD Biosciences) into complete DMEM media before RNA extraction.

Image analysis. Images from confocal microscopy and from two-photon microscopy were analysed on either Velocity software (Improvision) or Imaris (Bitplane).

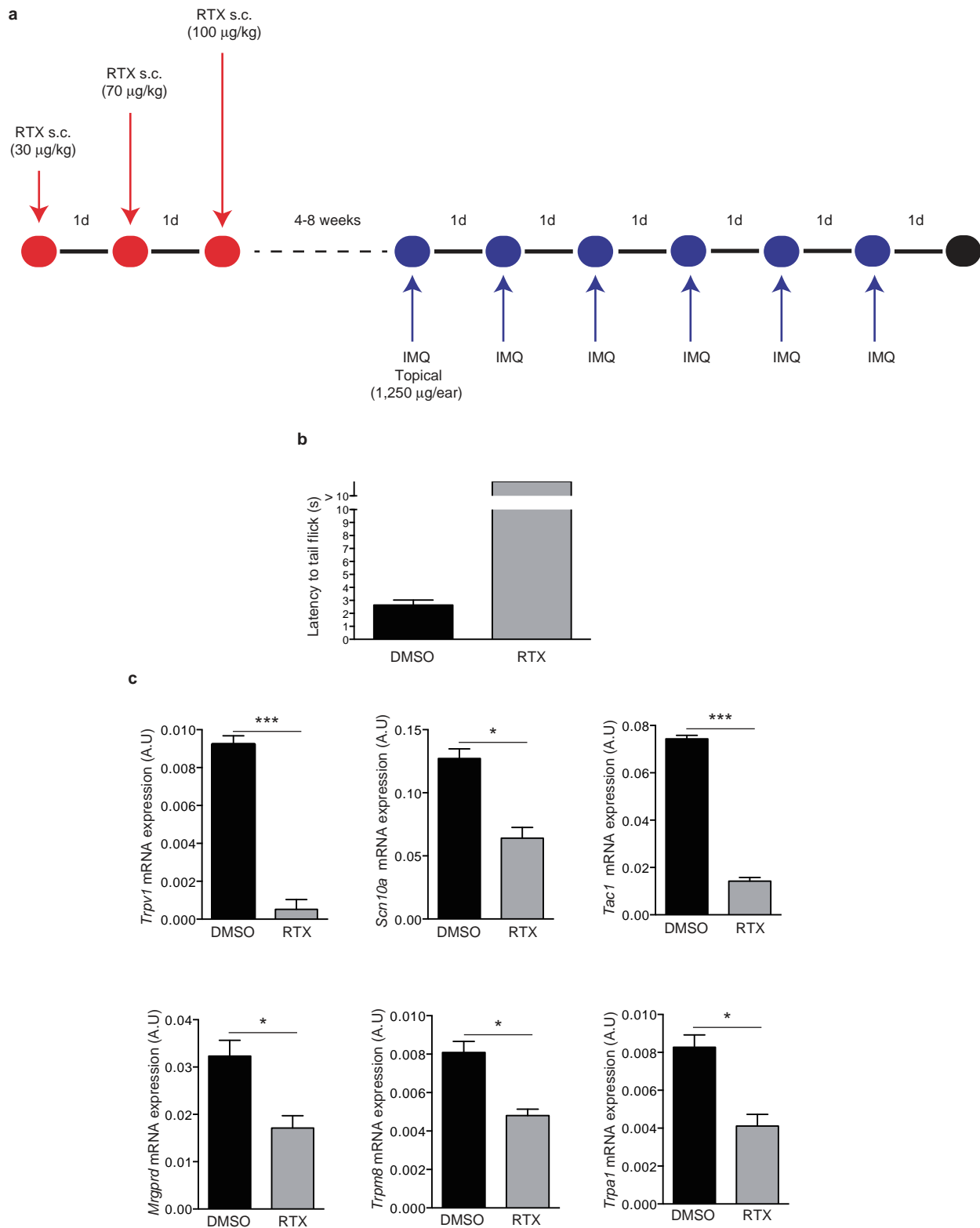
For determining the distance of CD11c-YFP cells from nerves, lymphatics or blood vessels, the centroid of dendritic cells was calculated by an unbiased approach, and the distance between a given dendritic cell centroid and the closest nerve, blood vessel or lymphatic vessel was calculated using Imaris software. To bin cells into contact (<0 μ m), proximal (0–7 μ m) and distal (>7 μ m) fractions, the calculated average radius of a dendritic cell (7.04 μ m) was subtracted from each measured distance. **Statistical analyses.** Precise experimental numbers of animals are reported in the figure legends. Experiments were repeated at least three times except in Figs 2e and 3e–g in which two replicates were done assessing ten mice total in each experimental group overall. Some data, such as ear-swelling curves, represent pooled averages of the sum total of animals used in experiments whereas other data consist of a representative experiment of the independent experiments. All statistical analyses were performed using Prism (GraphPad Software) and results are calculated as means with error bars representing the s.e.m. Means between two groups were compared by using a two-tailed *t*-test. Means between three or more groups were compared by using a one-way or two-way ANOVA. A Chi-squared statistical analysis was performed for Fig. 4d comparing the total number of dendritic cells in contact, proximal and distal bins relative to nerves versus lymphatic vessels or versus blood vessels.

31. Lindquist, R. L. *et al.* Visualizing dendritic cell networks *in vivo*. *Nature Immunol.* **5**, 1243–1250 (2004).
32. De Togni, P. *et al.* Abnormal development of peripheral lymphoid organs in mice deficient in lymphotoxin. *Science* **264**, 703–707 (1994).
33. Jung, S. *et al.* *In vivo* depletion of CD11c⁺ dendritic cells abrogates priming of CD8⁺ T cells by exogenous cell-associated antigens. *Immunity* **17**, 211–220 (2002).
34. Garcia, A. D., Doan, N. B., Imura, T., Bush, T. G. & Sofroniew, M. V. GFAP-expressing progenitors are the principal source of constitutive neurogenesis in adult mouse forebrain. *Nature Neurosci.* **7**, 1233–1241 (2004).
35. Boes, M. *et al.* T-cell engagement of dendritic cells rapidly rearranges MHC class II transport. *Nature* **418**, 983–988 (2002).
36. Saito, M. *et al.* Diphtheria toxin receptor-mediated conditional and targeted cell ablation in transgenic mice. *Nature Biotechnol.* **19**, 746–750 (2001).



Extended Data Figure 1 | 6OHDA treatment ablates sympathetic nerve function and reduces ear swelling, but does not ameliorate the inflammatory response to IMQ treatment. **a**, The experimental protocol was as follows. Mice were injected intraperitoneally with 6OHDA, resulting in a reversible chemical sympathectomy lasting for approximately 2 weeks. After a rest period of 3 days animals were challenged topically on the ear with IMQ. **b**, Representative section of splenic white pulp showing B cells (B220, white), T cells (CD3, red), and TH⁺ (green) nerve fibres in vehicle

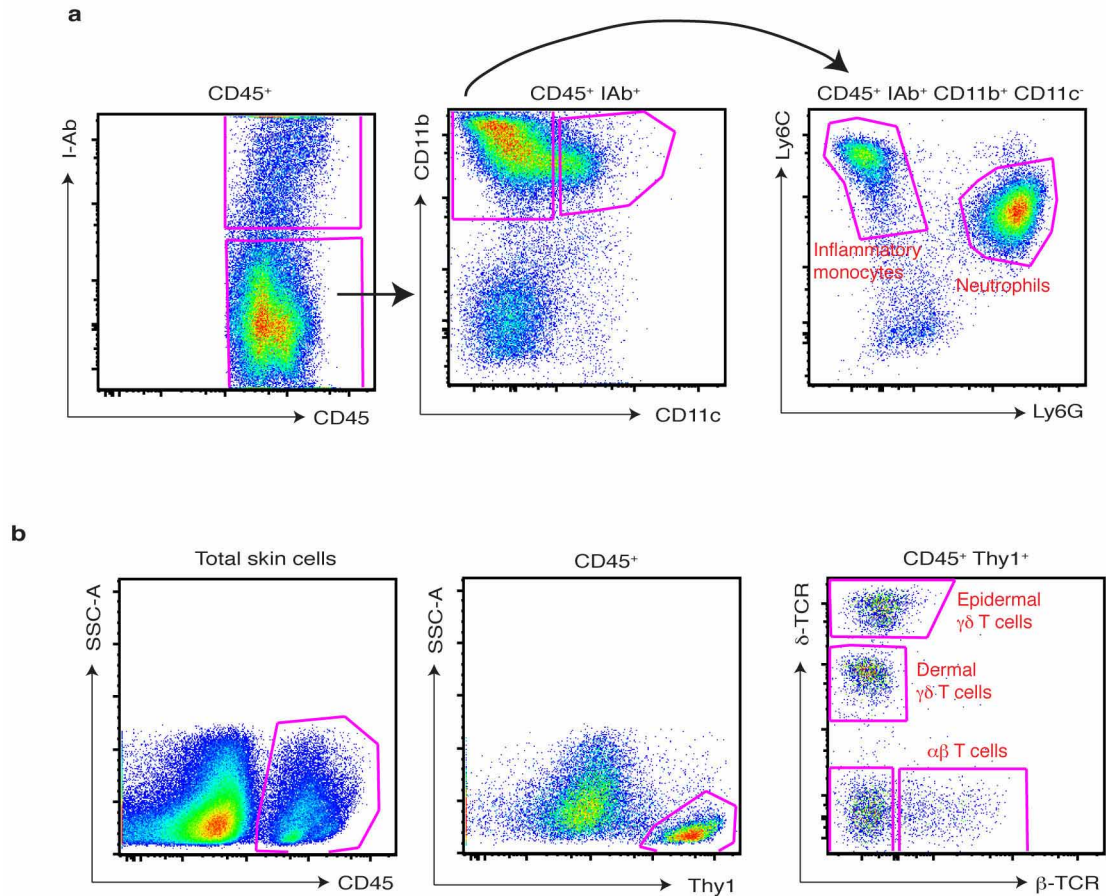
(ascorbic acid)-treated and sympathectomized (6OHDA) mice. **c–i**, Analysis of the inflammatory response in ears of vehicle (ascorbic acid)-treated and sympathectomized (6OHDA) mice after daily topical IMQ challenge: timecourse of change in ear thickness of IMQ-treated ear relative to the contralateral ear ($n = 10$; $*P < 0.05$; $**P < 0.01$) (**c**) and total number of infiltrating monocytes (**d**) and neutrophils (**e**), and the amount of IL-17A (**f**), IL-17F (**g**), IL-22 (**h**) and IL-23p40 (**i**) in protein extracts of IMQ exposed ears at day 3 ($*P < 0.05$; $n = 5$). NS, not significant.



Extended Data Figure 2 | RTX treatment diminishes noxious heat sensation and decreases the expression of nociceptor markers on dorsal root ganglia.

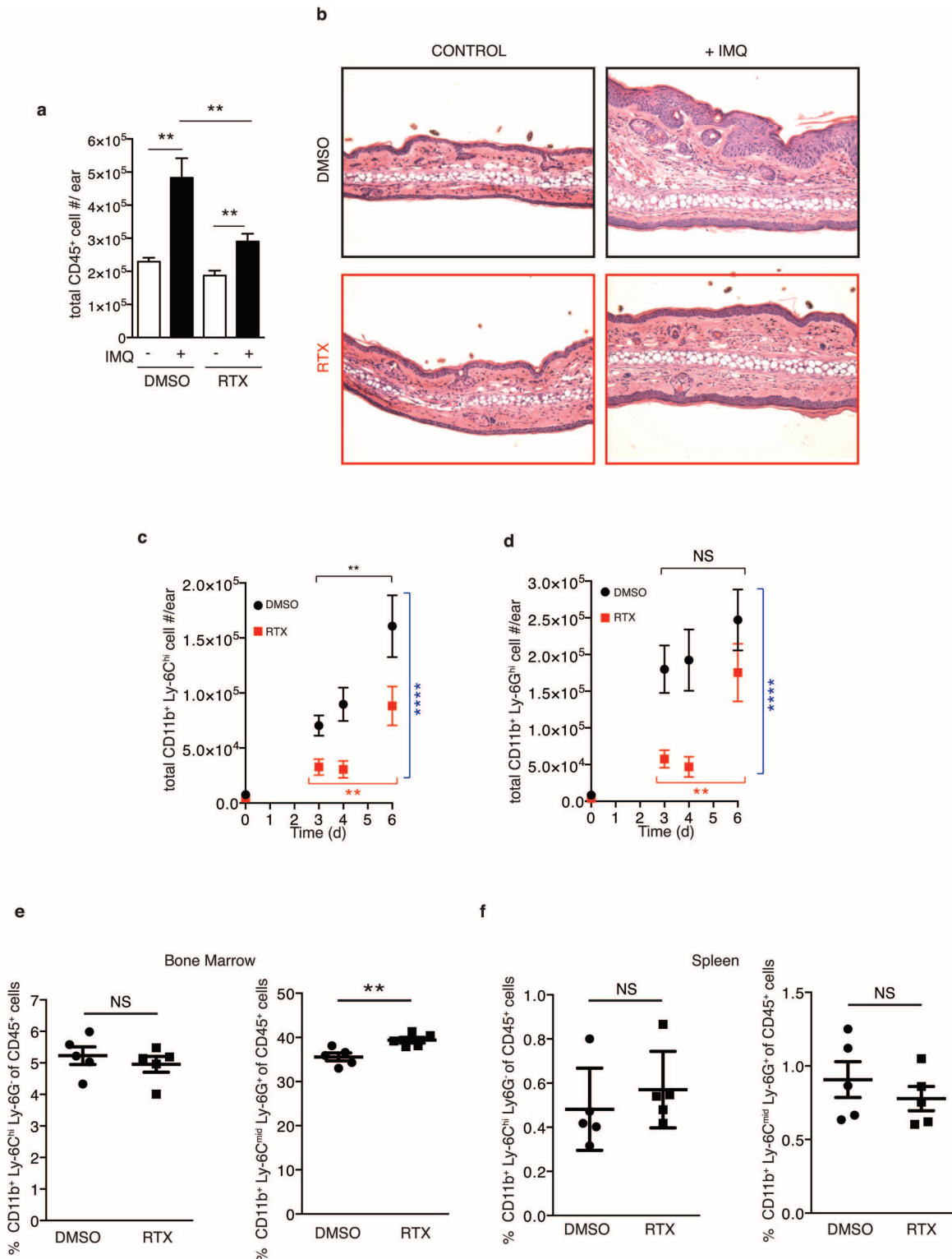
a, Schematic protocol of nociceptor ablation and induction of psoriasiform skin inflammation. RTX was injected subcutaneously into the back in three escalating doses ($30 \mu\text{g kg}^{-1}$, $70 \mu\text{g kg}^{-1}$ and $100 \mu\text{g kg}^{-1}$) on consecutive days and mice were allowed to rest for at least 4 weeks before IMQ treatment.

b, Denervation was confirmed by immersing the tail of mice into a temperature-controlled water bath maintained at 52°C and the latency to the first tail movement to avoid water was measured ($n = 6$). **c**, Total RNA was isolated from dorsal root ganglia (level C1–C7) of vehicle (DMSO)- and RTX-treated mice and the levels of *Trpv1*, *Scn10a* ($\text{Na}_v1.8$), *Tac1* (substance P), *Mrgprd*, *Trpm8* and *Trpa1* mRNA relative to *Gapdh* were determined ($n = 3$).



Extended Data Figure 3 | Gating strategy for myeloid cells and T-cell subsets from digested ear skin. **a**, The ear skin of mice challenged for 3 days with IMQ was digested as described in Methods and, after doublet exclusion and gating on defined FSC-A, SSC-A parameters, infiltrating myeloid cells were gated as $CD45^+ I\text{-Ab}^-$ (Class-II) $^-$, $CD11b^+ CD11c^-$, and then subdivided into

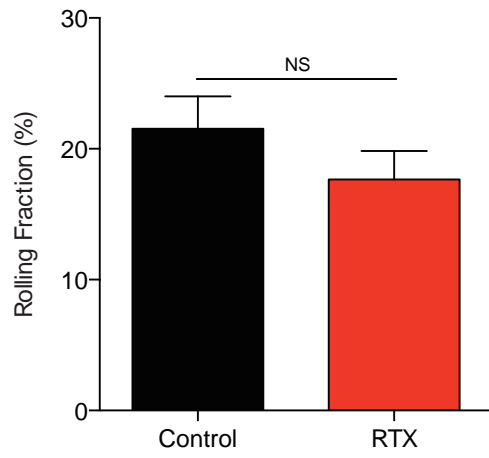
inflammatory monocytes and neutrophils based on Ly-6C and Ly-6G staining. **b**, The ear skin of naive mice was digested as described in Methods and, after doublet exclusion and gating on defined FSC-A, SSC-A parameters, cutaneous T cells were gated on $CD45^+$, $Thy1^+$, and then divided into subsets based on staining for δ -TCR and β -TCR.



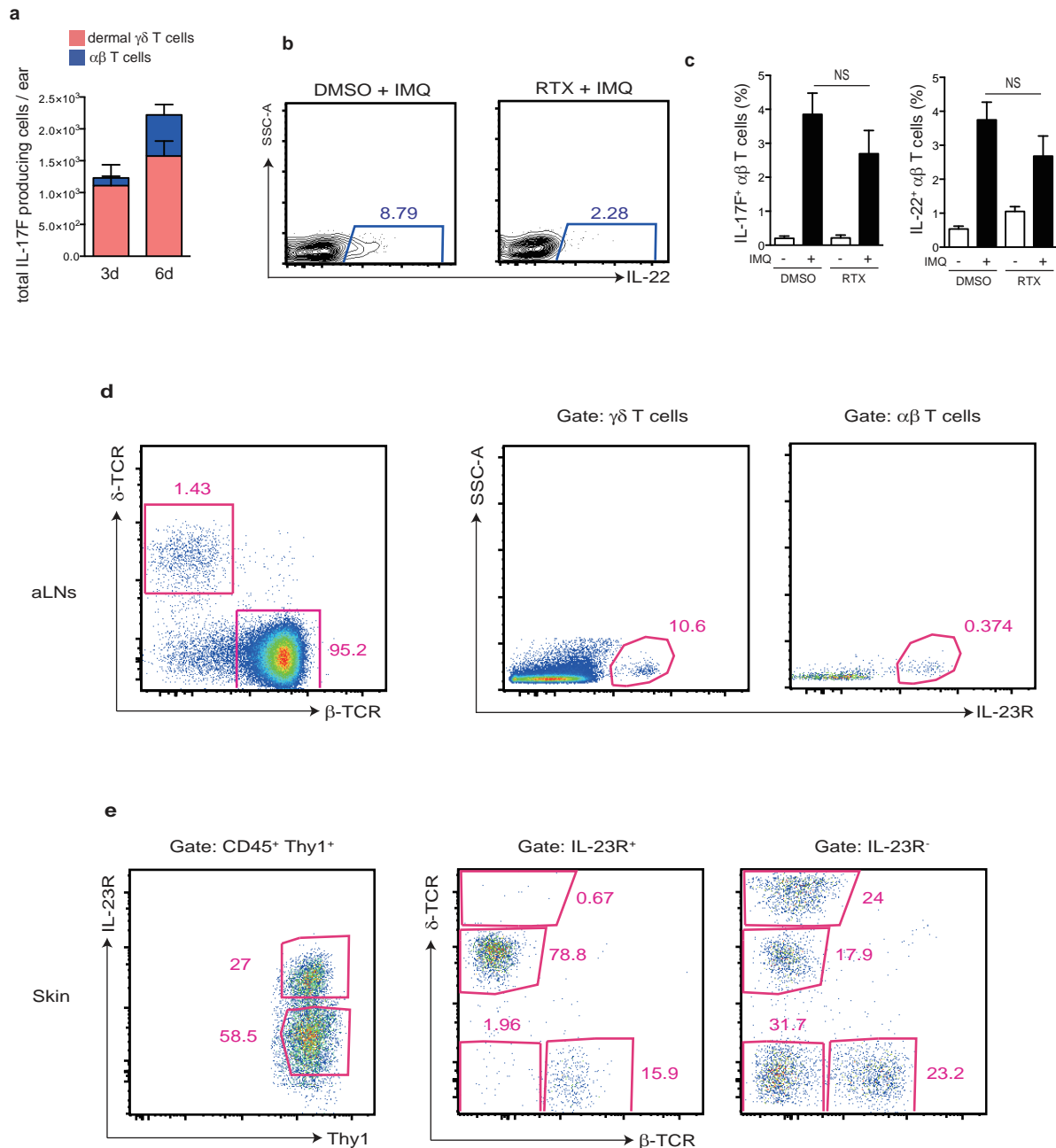
Extended Data Figure 4 | RTX treatment reduces the immune cell infiltrate upon IMQ treatment in the skin but does not affect reservoirs of inflammatory monocytes and neutrophils at steady state.

a, The ear skin of untreated (DMSO) or sensory denervated (RTX) mice was treated with topical IMQ cream daily and the total numbers of CD45⁺ cells were determined on day 3 as explained in Methods ($n = 10$). **b**, Representative histological sections of untreated and IMQ-treated ears at day 3 stained by haematoxylin and eosin ($\times 20$) ($n = 5$ per condition). **c**, **d**, Total inflammatory monocytes (CD45⁺, CD11b⁺, Ly-6C^{high}) and neutrophils (CD45⁺, CD11b⁺, Ly-6G^{high}) were determined by flow cytometry ($n = 5$ –10 mice per time point). Two-way ANOVA was run to compare total numbers of inflammatory monocytes and

neutrophils between DMSO and RTX conditions over days 3–6 (**** $P < 0.0001$). One-way ANOVA was run to compare total inflammatory monocytes and neutrophil numbers over days 3–6 within DMSO or RTX conditions (** $P < 0.003$). **e**, Bone marrow was isolated from wild-type and RTX mice from one femur and the frequency of inflammatory monocytes (CD45⁺, CD11b⁺, Ly-6C^{high}, Ly-6G⁻) and neutrophils (CD45⁺, CD11b⁺, Ly-6C^{mid}, Ly-6G⁺) relative to CD45⁺ cells was determined by flow cytometry ($n = 5$). **f**, Spleens from wild-type and RTX mice were processed for flow cytometry and the frequency of inflammatory monocytes (CD45⁺, CD11b⁺, Ly-6C^{high}, Ly-6G⁻) and neutrophils (CD45⁺, CD11b⁺, Ly-6C^{mid}, Ly-6G⁺) relative to CD45⁺ cells was determined ($n = 5$). NS, not significant.

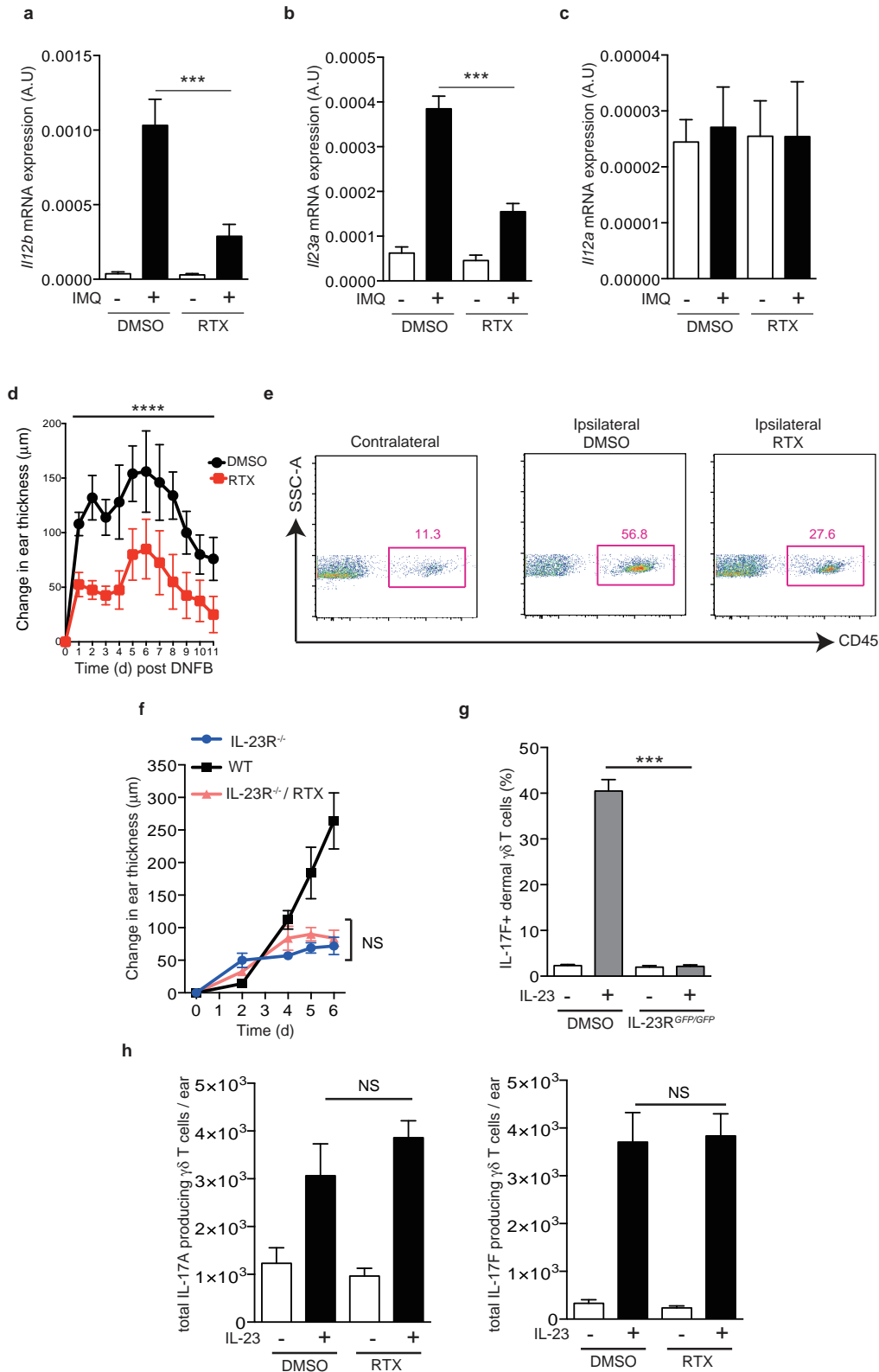


Extended Data Figure 5 | Leukocyte rolling fractions in skin venules of control and RTX-treated mice analysed by intravital microscopy. Combined results are shown for 26 venules from 5 control mice and for 20 venules from 4 RTX-treated mice. Data are expressed as mean \pm s.e.m. of four experiments. NS, not significant.



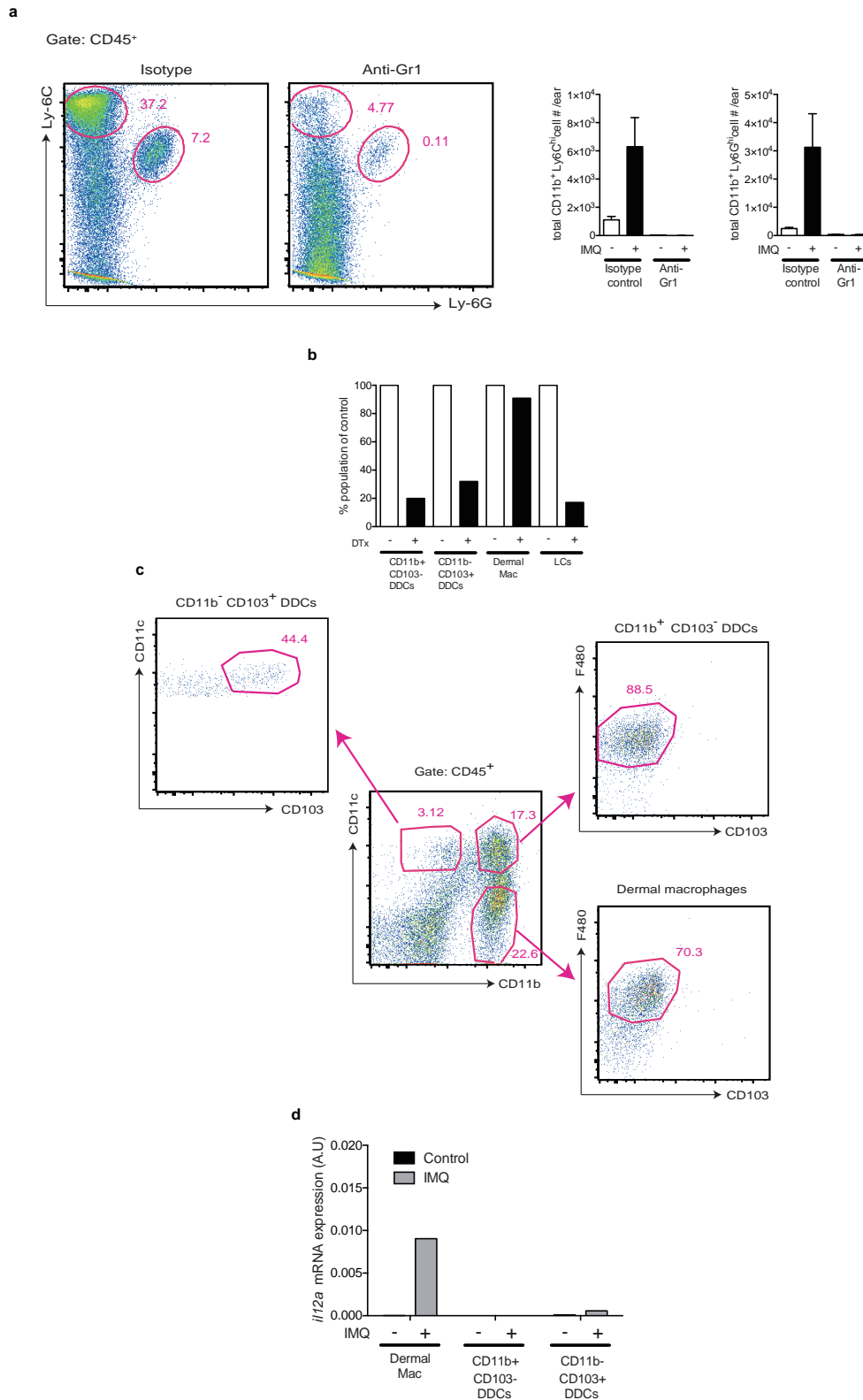
Extended Data Figure 6 | Dermal $\gamma\delta$ T cells represent a major source of IL-17F and IL-22 in skin during IMQ challenge and already express IL-23R at steady state. **a**, Wild-type mice were challenged with IMQ and the total numbers of IL17F⁺ dermal $\gamma\delta$ T cells and $\alpha\beta$ T cells at 3 days ($n = 15$) or 6 days ($n = 10$) were quantified. **b**, Representative flow plots (related to those depicted in Fig. 2g) of gating for IL-22⁺ cells within dermal $\gamma\delta$ T cells after 6 days of IMQ treatment. **c**, Ears of DMSO- or RTX-treated mice were exposed for 6 days to IMQ and the frequency of IL-17F⁺ and IL-22⁺ cells within $\alpha\beta$ T cells was

determined ($n = 5$). **d**, Auricular lymph node (aLN) cells from IL-23R^{GFP/+} mice were analysed by flow cytometry for expression of IL-23R-GFP⁺ cells within the $\gamma\delta$ T cells and $\alpha\beta$ T cell compartment at steady state (representative FACS plot from eight mice analysed). **e**, The ear skin from IL-23R^{GFP/+} mice was digested and analysed by flow cytometry and the distribution of T-cells subsets within IL-23R-GFP⁺ and IL-23R-GFP⁻ fractions of Thy1⁺ cells determined (representative FACS plot from eight mice analysed). NS, not significant.



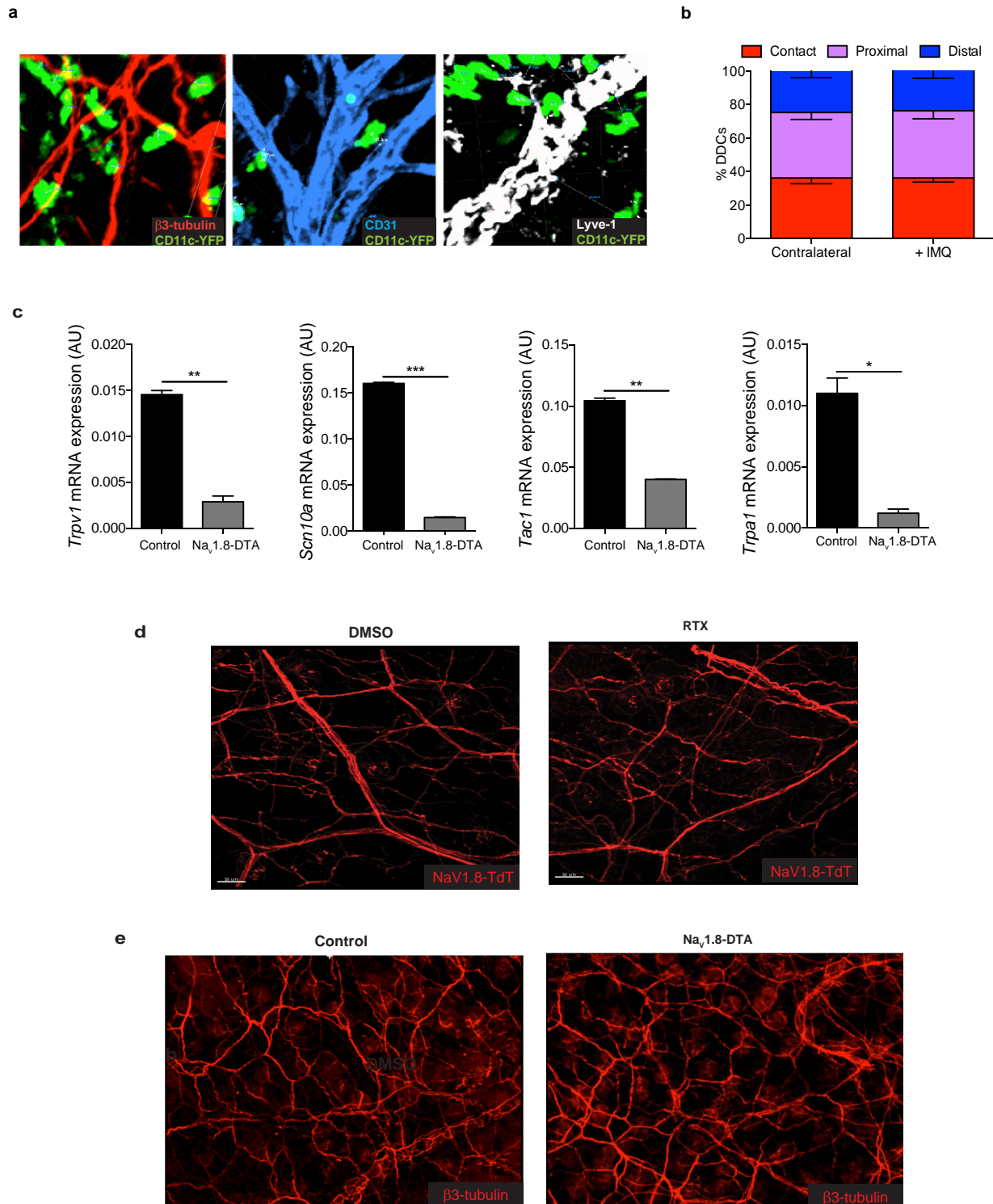
Extended Data Figure 7 | TRPV1⁺ nociceptors regulate IMQ- and DNFB-induced dermatitis and are upstream of IL-23. a–c, After 3 days of IMQ challenge, ears were harvested and processed for total RNA isolation and *Il12b* (a), *Il23a* (b) and *Il12a* (c) mRNA levels were analysed by qPCR ($n = 5$). d, DNFB (0.5% in acetone) was applied topically to DMSO and RTX mice. Time course of change in ear thickness of IMQ-treated ear relative to the contralateral ear is represented ($n = 10$). Two-way ANOVA was run to compare ear swelling under DMSO and RTX conditions over time ($****P < 0.0001$). e, Representative FACS plots from ears harvested after 24 h

of DNFB application. f, IL-23R^{GFP/GFP} mice were treated with RTX and then compared to wild-type and IL-23R^{GFP/GFP} littermate controls during IMQ treatment. Ear thickness was calculated relative to the contralateral ear ($n = 5$). g, After two IL-23 injections into the ear skin of wild-type and IL-23R^{GFP/GFP} mice, the frequency of IL-17F⁺ cells within dermal $\gamma\delta$ T cells was determined by flow cytometry ($n = 5$). h, IL-23 was injected twice into the ear skin of vehicle- and RTX-treated mice and the total numbers of IL17A⁺ or IL-17F⁺ dermal $\gamma\delta$ T cells per ear were determined by flow cytometry ($n = 5$). NS, not significant.



Extended Data Figure 8 | Selective depletion of migratory and skin-resident myeloid cell subsets in ear skin and gating strategy used for sorting to isolate RNA from MHC-II⁺ cells in skin. **a**, Wild-type mice were treated with anti-Gr-1 (clone RB6-8C5 to deplete neutrophils and inflammatory monocytes) or matched isotype control, challenged with IMQ for 3 days and skin was digested to quantify the total numbers of inflammatory monocytes and neutrophils per ear. Shown are representative plots pre-gated on CD45⁺ cells and quantification of cell numbers from $n = 3$ mice. **b**, DTX treatment resulted in depletion of both subsets of DDCs as well as Langerhans cells (LCs)

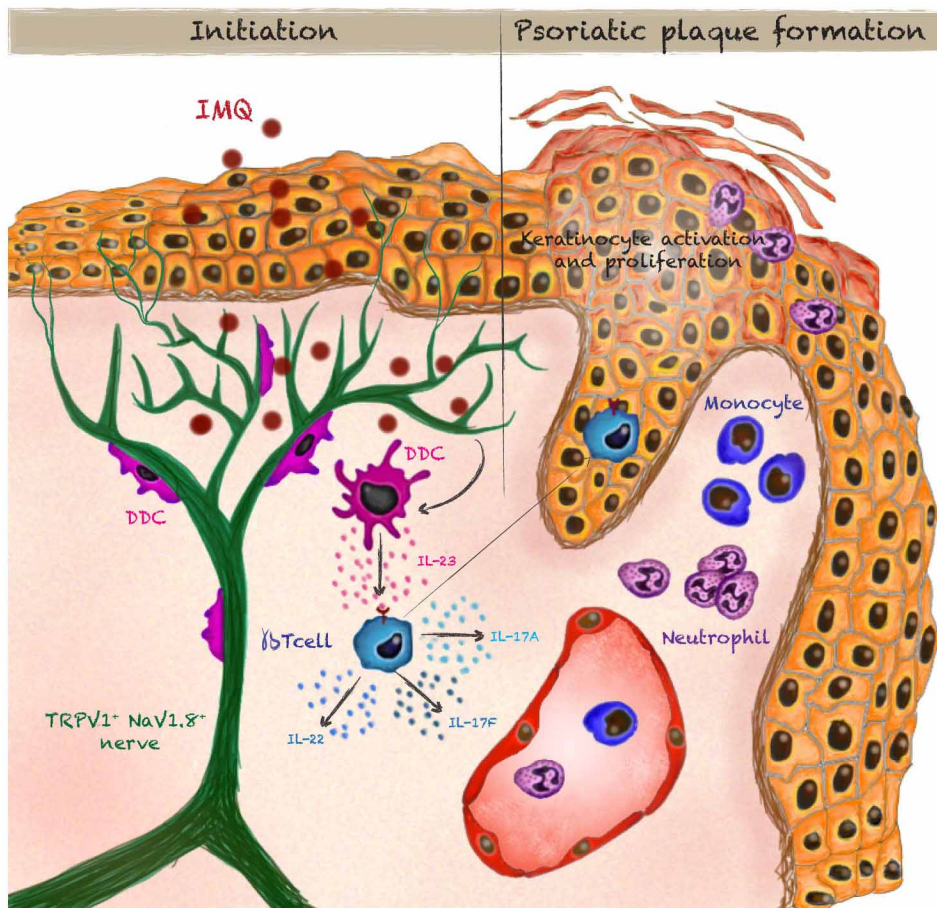
but not macrophages. Cells were gated as shown in Extended Data Fig. 8c and normalized to levels in wild-type mice based on the frequency within the CD45⁺ population from $n = 4$ mice. **c**, Ear skin from naive mice was digested and analysed by flow cytometry for the indicated subsets. Shown is a representative plot pre-gated on CD45⁺ Class II⁺ cells from which further subsets were divided based on CD11b and CD11c expression and then F4/80 and CD103 as indicated. **d**, Total RNA from sorted cells was isolated and qPCR for *Il12a* relative to *Gapdh* was performed from naive and IMQ-treated ears after 6 h from $n = 20$ pooled mice.



Extended Data Figure 9 | DDCs are found in close apposition to Na_v1.8⁺ nociceptors and characterization of RTX-treated and Na_v1.8-DTA mice.

a, Representative confocal micrographs of CD11c-YFP mice stained for β3-tubulin, Lyve-1 (lymphatics) and CD31 (blood and lymphatic endothelial cells). **b**, Three-dimensional quantification of DDC proximity to peripheral nerves in naive and 6 h post-IMQ treatment ears binned into contact (<0 μm), proximal (0–7 μm) and distal (>7 μm) fractions as explained in Methods (*n* of dendritic cells = 200). **c**, Total RNA from dorsal root ganglia (C1–C4) of littermate control and Na_v1.8-DTA mice was isolated and levels of mRNA for *Trpv1* (TRPV1), *Scn10a* (Na_v1.8), *Tac1* (substance P) and *Trpa1* (TRPA1) were

determined relative to *Gapdh*. This demonstrates the efficacy of the Na_v1.8-DTA system and combined with the original reference characterizing the pain phenotype of these mice illustrates that a subset of peptidergic TRPV1⁺ nerve fibres is spared. **d**, Representative confocal micrograph of whole-mount ear skin of vehicle- and RTX-treated mice showing preserved nerve scaffold. **e**, Representative confocal micrographs of whole-mount ear skin of control and Na_v1.8-DTA mice showing preserved nerve scaffold. Although dorsal root ganglia showed a loss of the hallmark ion channels of these nerve subsets (Extended Data Figs 1c, 9c), surprisingly we still observed that RTX mice and Na_v1.8-DTA mice maintain a meshwork of nerves in the skin.



Extended Data Figure 10 | Summary diagram.